General DAB 1 st Harmonic TPS State Space Model

Simon Uicich, Jean-Yves Gauthier, Xuefang Lin-Shi, Bruno Allard, Arnaud Plat

General DAB 1^{st} Harmonic TPS State Space Model

Uicich, Simon[1] Gauthier, Jean-Yves [2] Lin-Shi, Xuefang[2] Allard, Bruno[2] Plat, Arnaud[3]

***Abstract*—This paper proposes a generalized averaging 1^{st} harmonic state space model for Dual Active Bridge (DAB) converters fitting any triple phase-shift (TPS) modulation as well as classical modulation schemes. The model provides an analysis about steady state and AC behavior and about operating characteristics like RMS current and conducted emissions. Comparison of results with a full order SPICE simulation show a good agreement as well as with regard to the dynamic behavior prediction. With TPS modulation being the most effective means for optimizing the DAB's efficiency, the proposed approach avoids classical implementations' typical drawbacks such as the need for multiple models corresponding to the mapping of different operating space regions with respect to modulations or the need to pre-constrain control variables to specific switching modes. It can also help reduce the impact of large signal transients on the output filter or of the converter performance degradation with aging. The proposed model is suitable for designing a non-linear control scheme allowing better converter performances in relation to a classical one. The interest and accuracy of the proposed approach are shown through a 150W, 28V to 12V DAB design used for a flight computer power supply where the versatility in controller design and the converter efficiency optimization are required.**

***Index Terms*—DAB, Model, triple phase-shift modulation, 1^{st} harmonic state space modeling**

I. Introduction

As in most classical converters, the Dual Active Bridge (DAB) uses a reactive (inductive) element to connect two voltage sources (input and output buses in Fig. 1). A transformer between these two buses provides galvanic isolation. The converter power flow is controlled through the phase-shift between each of its bridge' legs.

From a broader converter level perspective, the interest in using different modulation schemes (e.g. TPS, SPS, TRM, TZM, ESPS in Fig. 2) is that they allow improving the converter efficiency. SPS stands for Simple Phase Shift Modulation, TZM for Trapezoidal Current modulation, TRM for Triangular current Modulation, ESPS to Extended Simple Phase-Shift Modulation.

1. Simon Uicich is with Airbus Operations, Toulouse (mail:simon.uicich@airbus.com) and with Univ Lyon, INSA Lyon, Université Claude Bernard Lyon 1, Ecole Centrale de Lyon, CNRS, Ampère, UMR5005, 69621 Villeurbanne, France (mail:simon.uicich@insa-lyon.fr).

2. Jean-Yves Gauthier, Xuefang Lin-Shi and Bruno Allard are with Univ Lyon, INSA Lyon, Université Claude Bernard Lyon 1, Ecole Centrale de Lyon, CNRS, Ampère, UMR5005, 69621 Villeurbanne, France (mails: jean-yves.gauthier@insa-lyon.fr, xuefang.shi@insa-lyon.fr, bruno.allard@insa-lyon.fr).

3. Arnaud Plat is with Airbus Operations, Toulouse, France (mail: arnaud.plat@airbus.com).

The modulation selection process consists partly in finding piece-wise analytical expressions relating each phase shift between each other and to system operating conditions (input/output voltage and load) so as to minimize losses [1], [3], [4]. A distinct discrete-time model is then needed for control design under each modulation, with precise mapping of the operating space required. This requires more design time and application processor memory and a longer control routine. It also means that when the converter must transition from one operating region to another one changing the modulation type, it could be harder to control large signal transients. On the other hand, the closed-loop control of converter current that the model could allow, is a key feature for maintaining the converter's performance over a long lifetime application with varying system parameters. Moreover, a unified model/control approach avoids large signal transients that can occur in adaptive modeling and may impact negatively the output filter size or the processing load.

This introduction presented the need for the DAB model's development. Section II will present the modeling approach in contrast with existing alternatives. Section III will develop the corresponding equations for triple phase-shift modulation. Section IV shows the insight into converter behavior obtained from the model and relevant to converter optimization such as the converter transfer function and frequency response, and estimations of the inductor RMS current, conducted emissions at the converter's input port or current amplitude at the switching instants inside the input bridge. Section V compares the converter behavior as described in Section III to the one from a full order simulation in power electronics simulation software PSIM.

II. Modeling Procedure

The DAB's main difference with respect to the classical voltage mode DC/DC converters is that mean current in the reactive element is null. Thus, classical state space averaging is not capable of describing all of the state's important large

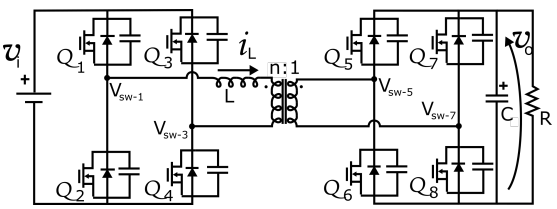

Fig. 1. Schematic of the DAB converter with relevant signals: inductor current - i_L-, output voltage -v_0- and i^{th} MOSFET associated switch node voltage V_{sw-i}, each one referenced to its respective ground (input or output).

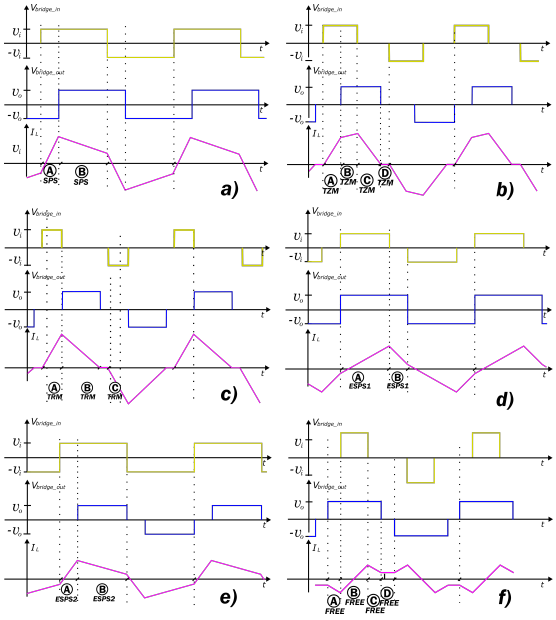

Fig. 2. Relevant waveforms associated to classic modulation approaches. a) Simple Phase Shift Modulation (SPS), b) Trapezoidal Current modulation (TZM), c) Triangular current Modulation (TRM), d) Buck Type Extended Simple Phase-Shift Modulation (ESPS1), e) Boost Type Extended Simple Phase-Shift Modulation (ESPS2), f) An arbitrary free TPS modulation.

signal behavior. So, to determine the control-to-output transfer function needed for output voltage/power flow regulation, a discrete-time approach similar to state space averaging the segmented analytical method (SAM) [2] is often used as in [1],. This discrete time approach analyses the evolution of states throughout a switching period while operating under a given switching mode [8], a specific sequence of switching period sub-intervals where the state of the power switches Q_1 to Q_8 is constant and thus the system behaves linearly (phase shifts being parameters). Constant output voltage is assumed to evaluate state evolution through each interval.

As an example, Fig. 3 shows relevant waveforms from a DAB controlled using a Triple Phase-Shift (TPS) Modulation. Note that the controllable delay between each leg's switching node voltage $d_i * T_{sw}$ is clearly marked. Each d_1, d_2, d_3 phase-shift configuration results in sub-intervals (A) to (D) beginning at t_A to t_D respectively. With the segmented analytical method (SAM), system dynamics at sub-interval (B) would be described as in (1).

$$\begin{bmatrix} \frac{di_L}{dt} \\ \frac{dv_0}{dt} \end{bmatrix}_B = \begin{bmatrix} 0 & -\frac{n}{L} \\ \frac{1}{C} & \frac{-1}{R \cdot C} \end{bmatrix} \cdot \begin{bmatrix} i_L \\ v_0 \end{bmatrix} + \begin{bmatrix} \frac{1}{L} \\ 0 \end{bmatrix} \cdot v_{in} \tag{1}$$

Thne state evolution along each sub-interval (B) can be developed as in [1] resulting in an expression like 2. Evaluating at $t = t_B$ gives the initial conditions for the following sub-interval (C), which has yet another state space model, and so on until $\mathbf{X}(t_A + T_{sw}) = f(\mathbf{X}(t_A))$, where $\mathbf{X} = [i_L, v_0]^T$, is found. This, together with the addition of an AC "small-signal" perturbation on control variables/states and linearization enables describing system dynamics with the Z transform.

However, note that the resulting model is limited to that specific sequence of power switch configurations, i.e. the different combinations of switch states result in different sub-interval descriptions. Fig. 2 shows different popular modulation types and their relevant waveforms. Thus, for example, the model based on Fig. 3 cannot represent Simple Phase-Shift (SPS) modulation in Fig. 2a, since sub-interval $(A)_{SPS}$ has no analog in Fig. 3 as it has no sub-interval for which the input bridge applies positive voltage while the output one applies negative voltage on L. In the same way, it cannot describe system behavior for an arbitrary free modulation as in Fig. 2e, since even if it has analog sub-intervals from $(A)_{FREE}$ to $(D)_{FREE}$, the sub-interval order is different, meaning different expressions for initial conditions result in an incompatible system description.

An alternative to this approach is the continuous time generalized averaged modelling method [9]. This was successfully formalized in [5] and applied to a DAB converter also in [6] [7], though limited to the particular case of SPS modulation. The focus here is modelling the dynamics of individual "time dependent" harmonics of system state variables, where a given k^{th} harmonic of an i^{th} state can be expressed with (3).

$$\langle x_i \rangle_k(t) = \frac{1}{T_{sw}} \int_{t-T_{sw}/2}^{t+T_{sw}/2} x_i(\tau) \cdot e^{-jk\omega_0 \cdot \tau} \cdot d\tau \tag{3}$$

Where $\omega_0 = 2 \cdot \pi / T_{sw}$. This means that the dynamics of a non linear system like $\frac{d}{dt}\mathbf{X} = F(\mathbf{X}, \mathbf{U})$, with frequency dependent behavior will be reduced to that of its n "time-varying" coefficients, considered as most important. Then, with respect to any k^{th} switching frequency harmonic, system dynamics can be described as $\langle \frac{d}{dt}\mathbf{X} \rangle_k = \langle F(\mathbf{X}, \mathbf{U}) \rangle_k$. The ultimate goal being to obtain the coefficients' dynamics: $\frac{d}{dt}\langle \mathbf{X} \rangle = F(\langle \mathbf{X} \rangle, \langle \mathbf{U} \rangle)$, where $\langle \mathbf{X} \rangle$ is the vector of the n "time-varying" coefficients of the system's m states, i.e.: $\langle \mathbf{X} \rangle(t) = [\langle x_1 \rangle_1(t), ..., \langle x_1 \rangle_n(t), ...\langle x_m \rangle_1(t), ..., \langle x_m \rangle_n(t)]$. A complete representation of a state will be as in (4), which can be differentiated to find the expression for the k^{th} coefficient of its derivative as in (5) where the first term of the right hand side contains the dynamics targeted by the model.

$$x(t) = \sum_{k=-\infty}^{\infty} \langle x \rangle_k(t) \cdot e^{j \cdot k \cdot \omega_0 \cdot t} \tag{4}$$

$$\langle \frac{d}{dt} x \rangle_k(t) = \frac{d}{dt} \langle x \rangle_k(t) + j \cdot k \cdot \omega_0 \cdot \langle x \rangle_k(t) \tag{5}$$

Since $F(\langle \mathbf{X} \rangle, \langle \mathbf{U} \rangle)$ can be non linear, i.e. it can contain the product of two signals, note its k^{th} coefficient can be calculated through convolution in the frequency domain as in (6) like for regular Fourier Series (FS).

$$\langle x \cdot y \rangle_k = \sum_{i=-\infty}^{\infty} \langle x \rangle_{k-i} \langle y \rangle_i \tag{6}$$

Generalized averaging as in (4) can also be analyzed as a conversion of higher frequency (HF) components to DC. This in turn allows one to evaluate the system behavior in

$$\begin{bmatrix} i_L(t) \\ v_0(t) \end{bmatrix}_B = \begin{bmatrix} (v_{in} - n \cdot v_0)/L \cdot (t - t_A) + i_L(t_A) \\ (v_{in} - n \cdot v_0)/L \cdot (t^2/2 - t_A * t + t_A^2/2)/C + (i_L(t_A) - v_0/R) \cdot (t - t_A)/C \end{bmatrix} \quad (2)$$

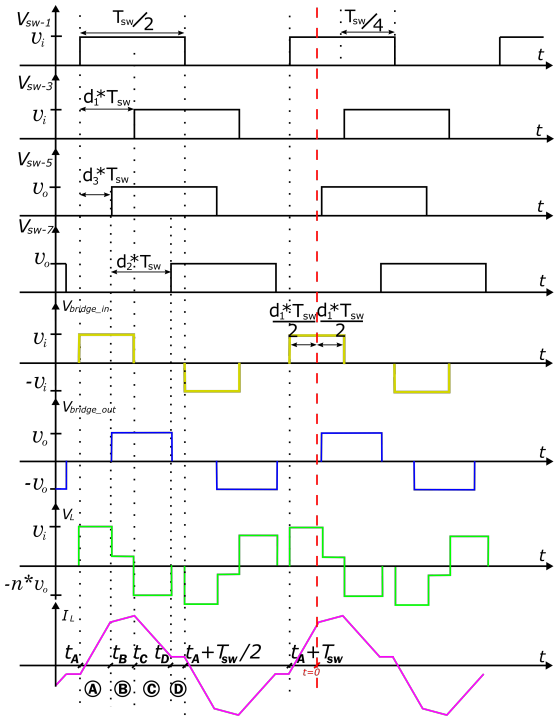

Fig. 3. Voltages at the switching nodes under Triple-Phase Shift modulation. V_{sw-i} relates to the i^{th} high-side MOSFET. The red dashed line marks time reference $t = 0$ for the model. V_{bridge_out} and V_{bridge_in} are the differential voltages $V_{sw-1} - V_{sw-3}$ and $V_{sw-5} - V_{sw-7}$ respectively. V_L (green) is the voltage applied across the inductor L

the frequency domain under a single frequency reference frame. As in average value state space modelling, an averaging operator is thereafter applied.

III. DAB Triple Phase-Shift Modulation 1^{st} Harmonic Model

Following the continuous time generalized averaged modelling procedure outlined in section II, for TPS modulation, an expression for $\langle \frac{d}{dt}\mathbf{X} \rangle_k = \langle F(\mathbf{X}, \mathbf{U}) \rangle_k$ should first be established. Through simple inspection of the circuit, the behavior in any sub-interval of the switching period can be described through (7) and (8)

$$C \cdot \langle \frac{dv_0}{dt} \rangle_k = \langle -v_0/R + i_L \cdot s_{out} \rangle_k - j \cdot k \cdot \omega_0 \cdot C \langle v_0 \rangle \quad (7)$$

$$L \cdot \langle \frac{di_L}{dt} \rangle_k = \langle v_{in} \cdot s_{in} - v_0 \cdot s_{out} - R_p \cdot i_L \rangle_k - j \cdot k \cdot \omega_0 \cdot L \langle i_L \rangle \quad (8)$$

Where R_p is a resistor in series with the inductor, partially representing losses in the converter. Also, s_{in} and s_{out} are switching functions taking values {-1, 0, 1} representing the state of either the power switches of each bridge, e.g. $s_{in}(t)$'s expression in the time domain being $sign(V_{sw-1}) - sign(V_{sw-3})$. While $V_{sw-3}(t) = V_{in} \sum_{n=-\infty}^{\infty} \Pi(\frac{2*(t-d_1*T_{sw}-n*T_{sw})}{T_{sw}})$. To proceed with the model development, the frequency expression of later functions need be crafted. Considering a time origin ($t = 0$) as in Fig. 3 for $V_{sw-1}(t) = V_{in} * s_{in,lead}$ the frequency expression of its time-varying expression will be:

$$\langle s_{in,lead} \rangle_k = \frac{sin(k \cdot \pi/2) \cdot e^{-j(\pi/2 + k \cdot \pi \cdot d_1)}}{k \cdot \pi}$$

Now considering the 2^{nd} input bridge leg is controlled analogously but shifted $d_1 * T_{sw}$, the input bridge's differential voltage can be written as:

$$\langle s_{in} \rangle_k = \frac{sin(k \cdot \pi/2) \cdot e^{-j(\pi/2 + k\pi d_1)} \cdot [1 - e^{-j2\pi k d_1}]}{k \cdot \pi} \quad (9)$$

Re-written as in (10).

$$\langle s_{in} \rangle_k = \frac{sin(k \cdot \pi/2) \cdot sin(\pi \cdot k \cdot d_1)}{k \cdot \pi/2} \quad (10)$$

Further, since s_{out} is delayed $(d_2/2 + d_3 - d_1/2) * T_{sw}$ with respect to $t = 0$ and the width of its rectangular pulses is $d_2 * T_{sw}$, it can be written as in (11).

$$\langle s_{out} \rangle_k = \frac{sin(k\pi/2) \cdot sin(k\pi d_2) \cdot e^{-jk\pi(d_2 - d_1 + 2d_3)}}{k\pi/2} \quad (11)$$

With the real and imaginary part of the first harmonic for each switching function being:

$$\langle s_{in} \rangle_{1r} = \frac{2 \cdot sin(\pi \cdot d_1)}{\pi} \quad (12)$$

$$\langle s_{out} \rangle_{1r} = \frac{2 \cdot sin(\pi \cdot d_2) \cdot cos(\pi \cdot (d_2 - d_1 + 2 \cdot d_3))}{\pi} \quad (13)$$

$$\langle s_{out} \rangle_{1i} = \frac{-2 \cdot sin(\pi d_2) \cdot sin(\pi (d_2 - d_1 + 2 \cdot d_3))}{\pi} \quad (14)$$

For the output voltage, being a DC/DC converter, the 0^{th} harmonic is being noted "v_0". For current "i_L", the approximation will be to model its behaviour through its first harmonic. Likewise, only the 1^{st} harmonic of the switching functions will be used. Note that all coefficients are to be decomposed in their real and imaginary parts to thereby enabling classic Laplace domain analysis. Applying (5), this reduces the system from (7) and (8) to (15), (16) and (17), where bracket notation is dropped for harmonics' representation. Note non-linearities are limited to the product of state variables with control variables.

$$C \frac{dv_0}{dt} = -v_0/R + 2 \cdot n \ (i_{L1r} s_{out,1r} + i_{L1i} s_{out,1i}) \quad (15)$$

$$L \cdot \frac{di_{L1r}}{dt} = v_{in} s_{in,1r} - n \cdot v_0 s_{out,1r} - R_p \cdot i_{L1r} + \omega_0 L \cdot i_{L1i} \quad (16)$$

$$L \cdot \frac{di_{L1i}}{dt} = -v_0 \cdot n \cdot s_{out,1i} - R_p \cdot i_{L1i} - \omega_0 \cdot L \cdot i_{L1r} \quad (17)$$

Despite the obtained system being readily controllable through the above-listed switching functions, to simplify analysis, they will be decomposed into the traditional phase-shift variables on which they depend and which are independent. Then, the system is linearized considering each state and phase-shift variables are the sum of the steady state and AC perturbation, $x_i = X_i + \tilde{x}_i$, $d_i = D_i + \tilde{d}_i$, resulting in $s_x = S_x + \tilde{s}_x$. Thus:

$$\begin{bmatrix} \tilde{s}_{in,1r} \\ \tilde{s}_{out,1r} \\ \tilde{s}_{out,1i} \end{bmatrix} = \begin{bmatrix} 2 \cdot \cos(\pi D_1) & 0 & 0 \\ 2 \cdot k_1 & 2(k_2 - k_1) & -4 \cdot k_1 \\ 2 \cdot k_3 & 2(k_4 + k_3) & -4 \cdot k_3 \end{bmatrix} \begin{bmatrix} \tilde{d}_1 \\ \tilde{d}_2 \\ \tilde{d}_3 \end{bmatrix} \quad (18)$$

Where $k_1 = \sin(\pi \cdot D_2) \cdot \sin(\Phi)$, $k_2 = \cos(\pi \cdot D_2) \cdot \cos(\Phi)$, $k_3 = \sin(\pi \cdot D_2) \cdot \cos(\Phi)$, $k_4 = \cos(\pi \cdot D_2) \cdot \sin(\Phi)$, $\Phi = \pi \cdot (D_2 - D_1 + 2 \cdot D_3)$. The resulting linearized system around steady-state operating point (V_{in}, V_0, I_L) is as shown in (19).

IV. Model Analysis

One first interesting aspect of the converter behavior that the model highlights is the allowable control space for any given operating point. A 150W, 28V to 12V DAB design used for a flight computer power supply is taken as an example. Fig. 4 plots D_1, D_2, D_3 combinations. The 2 degrees of freedom in control are clearly appreciated. Note that the "flattened-sphere-like" space is continuous, implying a continuous-time controller (e.g. PI) could suffice for directly controlling phase-shifts d_i.

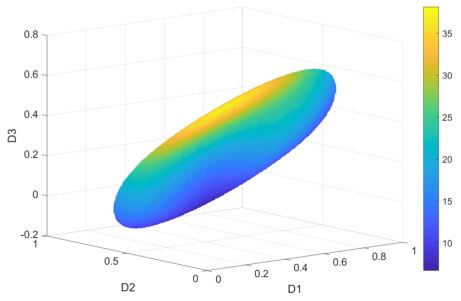

Fig. 4. Model allowable control space for 12V, 150W output at 28V input in a flight computer power supply. A cold to warm color gradient is used to represent the resulting RMS current in A.

On the other hand, it is interesting to show how a specific point in the resulting control space from the model performs with respect to classic modulations in terms of conduction loss. In this perspective, Fig. 5 shows transformer-primary winding RMS current throughout the operating space for classic modulations as well for a TPS-free modulation scheme that minimizes it. Note how the TPS-free modulation performs significantly better than classic modulations (30% less RMS current on average and up to 60% less current than the best classic modulation scheme). It should be noted however that for classic modulations, the standard relationship between each phase-shift values was used, with the controllable ones being determined through use of the model.

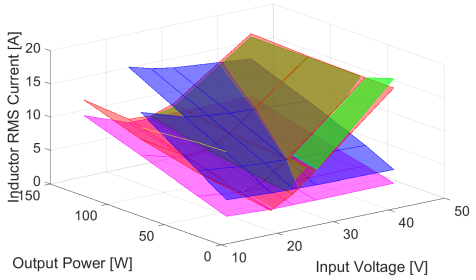

Fig. 5. Inductor RMS current throughout the operating space for SPS (red), TRM (blue), ESPS-buck (green), ESPS-boost (yellow), TPS-free (magenta) modulations.

Considering the impact EMI filters have on global power supply footprint, an interesting additional converter operating characteristic is the amount of AC current the power stage generates at the converter's input. Fig. 6 presents the values estimated using model state-variables and switching functions for both SPS, TRM and TPS-free modulations respectively resulting in the minimum RMS current. Once more, it is this last alternative that seems to have a slightly better performance, with worst case maximum conducted emissions at least 20% below the next-best classical modulation alternative.

One last characteristic of converter behavior awaited from the model is its AC behavior. Fig. 7 plots the gain of the transfer functions between each state-variable and control. Allocation of a specific control variable to command any state-variable can then be made accordingly, e.g. privileging control variables with more gain to command states with a faster dynamic, especially considering that different operating points were seen to impact low-frequency (LF) gains as much as $+/-20\,\mathrm{dB}$.

V. Model Validation

Comparing the model's response to specific control inputs both at DC and at certain frequencies to the one of a full order SPICE model allows one to directly evaluate the level of precision and thus its suitability for converter control, e.g. a reasonable rule of thumb could be to consider that its AC response in amplitude should not deviate more than 3dB and its phase response should be a few degrees accurate.

With the spirit of evaluating the model under the most "demanding" conditions, "hard" operating points were chosen, i.e. those for which the influence of higher order harmonics in the full order current waveform are supposedly the greatest. The operating points chosen as in Table I, with the input voltage, load resistance and modulation type with which the test was conducted, are shown in the first column.

$$\begin{bmatrix} \frac{d\tilde{v}_o}{dt} \\ \frac{d\tilde{i}_{L1r}}{dt} \\ \frac{d\tilde{i}_{L1i}}{dt} \end{bmatrix} = \mathbf{A} \cdot \begin{bmatrix} \tilde{v}_o \\ \tilde{i}_{L1r} \\ \tilde{i}_{L1i} \end{bmatrix} + \mathbf{B} \cdot \begin{bmatrix} \tilde{d}_1 \\ \tilde{d}_2 \\ \tilde{d}_3 \end{bmatrix}, \quad \mathbf{A} = \begin{bmatrix} -1/RC & 2 \cdot n \cdot S_{out,1r}/C & 2 \cdot n \cdot S_{out,1i}/C \\ -n \cdot S_{out,1r}/L & -R_p/L & \omega_0 \\ -n \cdot S_{out,1i}/L & -\omega_0 & -R_p/L \end{bmatrix}$$
$$\mathbf{B} = \begin{bmatrix} 4n \cdot (I_{L1r} \cdot k_1 + I_{L1i} \cdot k_3)/C & 4n \cdot (I_{L1r} \cdot (k_2 - k_1) + I_{L1i} \cdot (k_4 + k_3))/C & -8n \cdot (I_{L1r} \cdot k_1 + I_{L1i} \cdot k_3)/C \\ (V_{in} \cdot 2 \cdot \cos(\pi \cdot D_1) - V_0 \cdot n \cdot 2 \cdot k_1)/L & -V_0 \cdot n \cdot 2 \cdot (k_2 - k_1)/L & +V_0 \cdot n \cdot 4 \cdot k_1/L \\ -V_0 \cdot n \cdot 2 \cdot k_3/L & -V_0 \cdot n \cdot 2 \cdot (k_4 + k_3)/L & V_0 \cdot n \cdot 4 \cdot k_3/L \end{bmatrix} \tag{19}$$

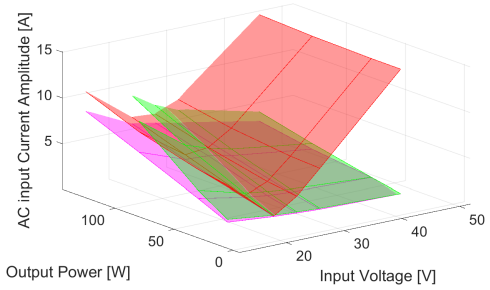

Fig. 6. Estimation of conducted emissions at converter input for SPS (red), TRM (green) and TPS-free (magenta) modulations.

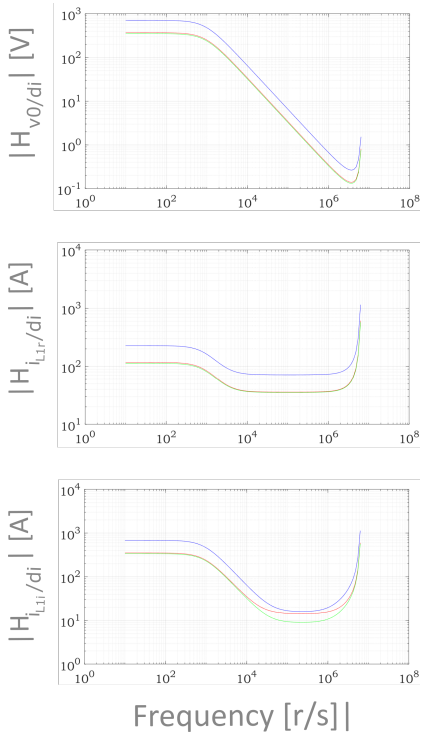

Fig. 7. Comparison of AC gain of state-variables with respect to each control variable $\tilde{d}_1$ (red), $\tilde{d}_2$ (blue), $\tilde{d}_3$ (green). The operating point is for $V_{in} = 28V, P_{out} = 150W$ with a TPS modulation minimizing transformer current.

As Table I shows, the large signal behavior fits the suitability criterion for both the output voltage, the control input and the real part of the transformer current. Note that when evaluating the modeling of TRM modulation, since there is a distinct unequivocal link between d_1 (the control variable D_{ctrl} in Table I) and v_0, the comparison was made in closed-loop

TABLE I

COMPARISON BETWEEN THE PROPOSED MODEL AND SPICE HIGH-ORDER CIRCUIT SIMULATION. AT EACH CELL, THE 1^{st} TO 3^{rd} LINES CONTAIN THE FULL ORDER SPICE SIMULATION VALUE/ THE MODEL ESTIMATED VALUE/ THE RELATIVE ERROR BETWEEN THEM.

V_{in}/R/Mod.	V_0	I_{L1r}	I_{L1i}	D_{ctrl}
16 V / 5.76 Ω / TRM		2.65 A / 2.83 A / 6%	−0.7 A / −0.87 A / 20%	0.149 / 0.153 / 2.6%
46 V / 5.76 Ω / TRM		1.6 A / 2.35 A / 45%	−0.3 A / −0.55 A / 77%	0.5 / 0.610 / 24%
46 V / 1.44 Ω / TRM		5.5 A / 5.9 A / 6%	−2.8 A / −2.7 A / 1%	0.10 / 0.102 / 1%
16 V / 5.76 Ω / Free-TPS	10.5 V / 11.5 V / 9%	1.15 A / 1.2 A / 5%	−0.45 A / 0.03 A / 93%	
28 V / 1.44 Ω / Free-TPS	12 V / 11.5 V / 5%	3.4 A / 2.9 A / 16%	−0.5 A / −1.3 A / 60%	
46 V / 1.44 Ω / Free-TPS	11 V / 11.5 V / 4%	3.1 A / 2.9 A / 7%	−1.8 A / −1.3 A / 38%	

operation, with v_0 regulated, and comparing the error between the model's predicted control variable value and the one obtained in SPICE simulation. It should be highlighted that the model results are worst for phase-shift values leading to high form factor current waveforms such as for TRM modulation with a 46 V input and a 25 W output load. The 5.76 Ω and 1.44 Ω values correspond respectively to 25 W and 100 W loads on the 12 V output voltage.

Further, the model can also be used to assess transient and small signal AC behavior useful for designing control schemes. In this sense a small step was applied on the control inputs and the state variable behavior was compared for both the proposed model and the SPICE circuit.

Fig. 8 shows the response of the model's states to a step of 1% of T_{sw} in the control input $\tilde{d}_3$. The error is limited to below 20% in steady state and for which converter dynamics are also properly represented. The most likely cause for the steady state deviation in the converter gain is the fact that only the first harmonic of the transformer current is considered. Note that the highly damped, short duration, high-frequency oscillations at the beginning of the transient in the models responses for current are intrinsic to the modeling approach and will not be detected by a low-frequency control routine. Even for other operating points using modulations for which the current transformer deviates from a sinusoidal waveform error in the step response was limited to less than 3 dB.

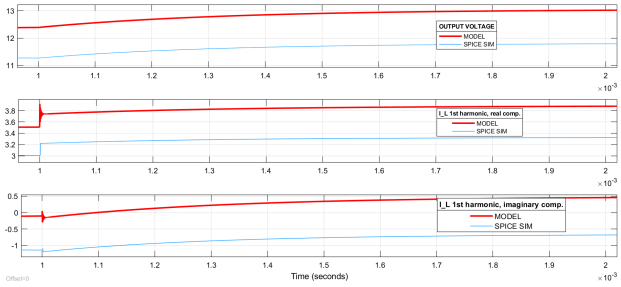

Fig. 8. 1^{st} Harmonic Model (blue) and SPICE simulation response (red) for a step in the control input $\tilde{d_3}$ when the converter is operating at 28V input voltage and with a 100W load with TPS modulation minimizing transformer 1^{st} harmonic RMS current.

Fig. 9 exemplifies the result of comparing the small-signal response of the proposed model with that of a real converter simulated through a SPICE-type simulator (PSIM) to an AC excitation of the phase-shift between both bridges ("$\tilde{d_3}$"). Note that at the frequency range of interest , i.e. below 15kHz - a feasible control frequency, the voltage error is below $6\,\mathrm{dB}$ and for a phase below $15°$. Further below 10kHz, the error is below $3\,\mathrm{dB}$ and $5°$. Similar results were obtained for the other two control variables and the other two state-variables for the operating points of interest, i.e. the steady state operating points for TPS-free modulations resulting in minimum RMS current in the first harmonic.

The last characteristic of the DAB's model that was evaluated was its ability to predict characteristics of interest opposite to performance optimization. These were: the transformer current RMS value and AC input current. In this sense, the simulation results were not encouraging since for Free TPS modulation, where the current waveform can drift further from a sinusoidal approximation, RMS values skewed more than 40% on some cases. For the case of unbalanced switching losses, this still allows a direct relative improvement of efficiency through using the said estimation. The reason is that in this case the error in the estimation of conducted losses does not make conduction losses comparable to other loss sources and so a variation in the control variables in order to improve losses can be foreseen. This was also true for the estimation of AC input current. However, for AC current, such a degree of precision could actually be interesting for input filter design optimization. Peak transformer current during the switching transitions was also evaluated having negligible correlation.

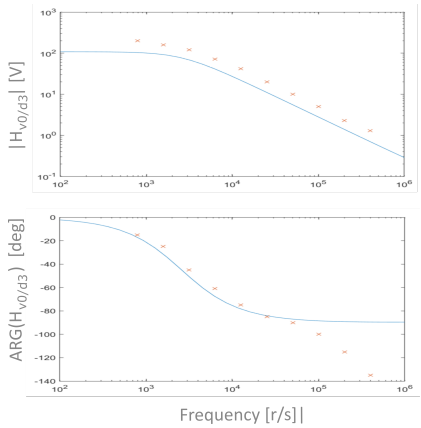

Fig. 9. Comparison between small-signal response of the simplified 1^{st} harmonic converter model (blue) and of a full-order simulation with PSIM (red) at 46V input voltage and 100W load with a free TPS modulation.

VI. Conclusions

To the authors' best knowledge, there was no model readily available for controlling the transformer current and output voltage in a DAB converter independently of the sub-type of triple phase-shift modulation. The generalized average first harmonic model of the DAB here developed provides an effective tool for doing this. The interest in a modulation independent approach is also shown in this paper, noting for example the 30% less RMS current with respect to using classical modulations that it allows. However, even if limited to classical modulation schemes, this model allows a quick allocation of specific modulations to different parts of the operating space, e.g. to minimize the transformer RMS current as in Fig. 5. In this perspective, the approach could be useful when searching to maximize DAB efficiency and integration in applications such as the one analyzed . An improvement to the model could be to also model the behavior of the 3^{rd} harmonic of the transformer current . The impact of the output capacitor ESR should also be assessed as in [5] to ensure proper system simplification.

References

[1] F. Krismer, "Modeling and optimization of bidirectional dual active bridge DC-DC converter topologies", ETH Zurrich PhD Thesis, 2010.

[2] Q. Gu, J. Nie, J. Sun, Z. Zhao, "Current Stress Minimization of Dual-Active-Bridge Covnerter Within the Whole Operating Range", IEEE Journal of Emerging and Selected Topics on Power Electronics, Vol. 7, No. 1, March 2019.

[3] G. G. Oggier, G. O. García, A. R. Oliva, "Modulation Strategy to Operate the Dual Active Bridge DC–DC Converter Under Soft Switching in the Whole Operating Range", IEEE Transactions on Power Electronics, Vol. 26, No. 4, April 2011.

[4] N. Hou, Y. Wei Li, "Overview and Comparison of Modulation and Control Strategies for Non-Resonant Single-Phase Dual-Active-Bridge dc-dc Converter", IEEE Transactions on Power Electronics, Vol. 35, No. 3, March 2020.

[5] H. Qin, J. W. Kimball, " Generalized Average Modeling of Dual Active Bridge DC-DC Converter", IEEE Transactions on Power electronics, Vol. 27, No. 4, Arril 2012.

[6] D-D Nguyen, G. Fujita, Q. Bui-Dang, M. C. TA, "Reduced-Order Observer-based Control System for Dual-Active-Bridge DC/DC Converter", IEEE Transactions on Industrial Applications, Vol. 54, No. 4, July-Aug. 2018.

[7] S. S. Shah, S. Bhattacharya, "Large and Small Signal Modeling of Dual Active Bridge Converter Using Improved First Harmonic Approximation", 2017 IEEE Applied Power Electronics Conference and Exposition (APEC), 26-30 March 2017.

[8] C. Calderon, A. Berrado, A. Rodriguez, P. Alou, A. Lozano, C. Fernandez, P. Zumel, "General Analysis of Switching Modes in a Dual Active Bridge with Triple Phase Shift Modulation", Energies, September 2018.

[9] I. Batarseh, K. Siri, "Generalized Approach to the Small Signal Modeling of DC-to-DC Resonant Converters", IEEE Transactions on Aerospace and Electronic Systems, Vol. 29, No. 3, July 1993.